LA-UR-12-00283

Approved for public release;
distribution is unlimited.

Title:	The MCNP6 Delayed-Particle Feature
Author(s):	Joe W. Durkee, Jr., Michael R. James, Gregg W. McKinney, Laurie S. Waters, and John T. Goorley
Intended for:	Publication in the Journal of Nuclear Technology

THE MCNP6 DELAYED-PARTICLE FEATURE

by

Joe W. Durkee, Jr., Michael R. James, Gregg W. McKinney,
Laurie S. Waters, and John T. Goorley
Los Alamos National Laboratory
jdurkee@lanl.gov
505-665-0530
Fax: 505-665-2897
PO Box 1663, MS K575
Los Alamos, NM 87545

ABSTRACT

The interaction of radiation with matter can cause activation or fission reactions with unstable residuals that decay with the emission of delayed-neutron and/or delayed-gamma radiation. This delayed radiation can be exploited for a variety of purposes, including homeland security, health physics, instrumentation and equipment design, and nuclear forensics. Here we report on capability that has been developed to provide automated simulations of delayed-neutron and/or -gamma radiation using MCNP6. We present new high-fidelity delayed-gamma simulation results for models based on the neutron-fission experiments conducted by Beddingfield and Cecil (1998) to illustrate and validate this powerful feature.

KEYWORDS: MCNP6; MCNPX; delayed gamma; delayed neutron; fission product; activation.

1. INTRODUCTION.

Use of computer simulations to examine complex phenomena continues to expand as hardware and software become increasingly sophisticated. In the arena of radiation transport, advances continue to be made that permit analyses with increasingly exquisite detail. Such detail can enable the inspection of subtle, yet important, processes and aspects of behavior.

Monte Carlo techniques provide analysts with a means to study radiation-transport phenomena that has a particularly high degree of fidelity. In the Monte Carlo paradigm, the interaction of radiation with matter is characterized by random sampling of the relevant processes. For the most part, simplifying limitations or approximations do not need to be placed on quantities such as particle energies, cross sections, directions, and spatial locations. Moreover, useful information can be generated regarding statistical behavior, and average values of quantities can be compared with experimental results.

Numerous radiation/matter-interaction processes have been identified, including activation and fission reactions. Our interest in this regard pertains to reactions that cause the production of unstable by-products ("residuals") that decay with half-lives ranging from seconds to years. The decay process is frequently accompanied by the emission of neutrons and photons. These particles are referred to as "delayed" to distinguish them from "prompt" neutrons and photons that are emitted virtually instantaneously following the nuclear reaction caused by the interaction of incident radiation and matter.

The emission of radiation caused by the decay of radioactive fission products has been of interest since the dawn of the nuclear age (Roberts et al., 1939; de Hoffmann, 1945; Moon, 1945). Delayed-neutron and -gamma applications are widespread and include health physics (Morgan and Turner, 1973; Szasz, 1984; Goudsmit, 1988), material assay (Hollas et al., 1987; Pruet et al., 2004; Norman et al., 2004**;** Slaughter et al., 2005), sensor protection (Spletzer, 1992), facility design (Henderson, et al., 1988; Liew and Ku, 1991; Guung et al., 2002) and calibration (Ma et al., 1996). Design of high-altitude instrumentation for environments involving hadronic interactions with radioisotope production and subsequent delayed-gamma emission also has gained importance (Weidenspointner et al., 2005) as has the characterization of nuclear was using delayed-gamma analysis (Dighe et al., 2009). Additionally, the detection of nuclear weapons and special nuclear material by means of active interrogation has evoked great interest in recent years (Siciliano et al., 2005; Dore et al., 2006; Sterbentz et al., 2007; Gozani T., 2009). Neutron-activation analysis (NAA) is a very active area of research that is being used in conjunction with active-interrogation techniques to detect explosives, chemical agents, and nuclear material (Barzilov et al., 2009; Chichester and Seabury, 2009). NAA involving prompt (PGNAA) and delayed gammas (DGNAA) is employed in radioanalytical chemistry, environmental, and health studies (Ayranov and Schumann, 2010; Fei et al., 2010; Frontasyeva et al., 2010).

The use of the Monte Carlo method for radiation transport began at Los Alamos National Laboratory (LANL) in the 1940s with a letter from John von Neumann to Robert Richtmyer, leader of the Theoretical Division at Los Alamos (von Neumann,

1947; Grant, 1989). John von Neumann estimated that execution of a calculation tracking 100 source neutrons through 100 collisions would require five hours using the ENIAC (Electronic Numerical Integrator and Computer), the world's first electronic computer! The letter to Richtmyer contained the first formulation of a Monte Carlo computation for an electronic computing machine. Since that time, LANL has developed and maintained Monte Carlo radiation-transport codes that have evolved into MCNP™ (Brown, 2003a; Brown, 2003b) and, prior to the merger, MCNPX™(Pelowitz, 2011). A merged version of MCNP and MCNPX, MCNP6, is expected to be released in early 2012.

MCNP6 (Goorley et al., 2012), like its recent predecessors, accommodates intricate three-dimensional geometrical models, continuous-energy transport of 34 different particle types plus heavy-ion transport, fuel burnup, and high fidelity delayed-gamma emission. MCNP6 is written in Fortran 90, has been parallelized, and works on platforms including single-processor personal computers (PCs), Sun workstations, Linux clusters, and supercomputers. MCNP has approximately 3000 users throughout the world working on endeavors that include radiation therapy, reactor design, and homeland security.

During the past few years, upgrades have been made to MCNPX and, as a result of the merger, MCNP6, which facilitate self-contained calculations with delayed-neutron (DN), delayed-gamma (DG), or delayed-neutron and delayed-gamma (DNDG) emission. The feature has been developed to make the delayed-particle feature as simple as possible to use, but provide the user with versatility and flexibility.

As part of the verification and validation effort for MCNP6, calculations have been performed to examine the delayed-particle feature. In this article we report results obtained using MCNP6 beta release version MCNP6_Release (load date November 28, 2011 version 6.2.24). The focus of this article is on the delayed-gamma validation work using models based on the experimental effort reported by Beddingfield and Cecil (1998) and augmented by data obtained during that effort that previously have not been reported.

In the following two sections the MCNP delayed-neutron and delayed-gamma data are discussed. An understanding of the content, amount, and availability of these data is important because they form the basis for the theoretical and computational structure of the MCNP DNDG feature. Section 4 presents several of the most prominent theoretical and computational attributes of the MCNP DNDG feature. In Section 5 we present some DG validation results.

2. MCNP DELAYED-NEUTRON EMISSION DATA.

Two techniques are implemented in MCNP6 to treat delayed-neutron emission. These techniques are called “library data” and “physics model.”

The library-data technique uses ACE (A Compact ENDF) data. This DN-production technique is available only for neutron-induced fission. Data are available for nuclides such as uranium and plutonium and for a number of energy groups that depend on the evaluation.

The physics-model technique can be used to produce DNs for fission or activation events induced by any source particle treated by MCNP. The total number of delayed neutrons produced by a fission or activation event is calculated using ENDF/B-VI delayed-neutron emission data (file cinder.dat). Sampling of the emission energies for DNs created by a fission or activation event is done using a set of pre-integrated emission probabilities that are cast in 750 energy groups for each of the 271 DN precursors (file delay_library.dat). These emission probabilities have recently been calculated (Kawano et al., 2008) based on the Quasiparticle Random Phase Approximation (QRPA) and the Hauser-Feshbach statistical model. Neutron emissions from an excited daughter nucleus after β-decay to the granddaughter residual are more accurately calculated than in previous evaluations that were done using a less sophisticated theoretical formulation (Kawano, 2011). The improved treatment includes all the microscopic nuclear structure information, such as a Gamow-Teller strength distribution and discrete states in the granddaughter. The calculated DN spectra agree reasonably well with those evaluations in the ENDF decay library, which are based on experimental data. The model was adopted to generate the delayed-neutron spectra for all 271 precursors if the ENDF decay data gives a simple evaporation spectrum.

3. MCNP6 DELAYED-GAMMA EMISSION DATA.

Delayed-gamma production by MCNP6 can be done only using the physics-model technique. There are no ACE data available to permit DG production by the library-data method.

The MCNP6 delayed-gamma emission-spectra data consist of two structures: multigroup and line data. All data are based on the ENDF/B-VI evaluation.

Of the two structures, the multigroup library is the more comprehensive dataset. These emission data are available in 25-group format for 3400 radionuclides, and the data reside in file cinder.dat (distributed with MCNP).

Line data have been obtained from the LANL Nuclear Information Service (located at http://t2.lanl.gov/data/data.html); these data have been extracted from the ENDF/B-VI evaluation. Radioactive-decay data for 979 radionuclides have been aggregated into the file cindergl.dat. These data include lower-energy photons, referred to as x-rays in these files. Throughout this article, the term "photon" is used interchangeably to connote gamma or x-ray, and the use of "gamma" is meant to include x-ray.

The line data comprise both discrete lines and "continuous" formats. The continuous data are evaluations at 10-keV intervals. For some radionuclides, all data are discrete; for others, it is continuous, and for the remainder, it is a combination of both discrete and continuous formats. Table 1 delineates the data composition.

The gamma-emission data reflect augmentation of measured ENDF/B-V data by calculated spectra (Katakura and England, 1991). The augmentation effort was conducted because reported measured emission data lacked a significant contribution of all gamma

rays emitted by fission products. In particular, it was noted that the measured decay-heat values exceeded calculated estimates. The disagreement was ameliorated by augmenting the measured data with calculated spectra based on theoretical models for all of the ENDF/B-V nuclides decaying by beta emission. The continuous data appear in the data files in the form of differential emission values with a 10-keV bin structure.

Table 1. Line-data composition for 979-radionuclide delayed-gamma dataset

Composition by Data Component		
Data component		**Quantity**
Total		282,035
Discrete		24,199
Continuous		257,836
File size (lines)		747,730
Composition by Nuclide		
Data component	**Nuclides**	**Quantity**
Discrete only	526 (54%)	19,821
Continuous only	292 (30%)	214,293
Discrete and continuous mix	161 (16%)	47,921 total 4378D, 67742C[a]

[a]D and C denote discrete and continuous data types.

The types and availability of DG data cause several important ramifications, and the MCNP6 DG feature has been developed accordingly. Major ramifications include (1) DG resolution, (2) execution speed, and (3) storage requirements. We have developed capability to do low- and high-resolution calculations. Extensive work has been done to maximize execution performance while simultaneously addressing the competing issue of storage requirement. These issues are examined in more detail in the following section.

4. MCNP6 DELAYED-PARTICLE TREATMENT.

The MCNP6 DNDG feature offers the user a large assortment of execution options. This feature also has been developed with capabilities to boost execution performance and limit storage requirements while being transparent to the user. To gain an understanding of these attributes, we first consider the general manner of DNDG procedure operations for the library-data and physics-model techniques.

4.1. DN library data procedure operation.

As discussed in Section 2, DN production for neutron-induced fission reactions can be done using the library-data technique. The general operation of this technique is illustrated in Fig. 1.

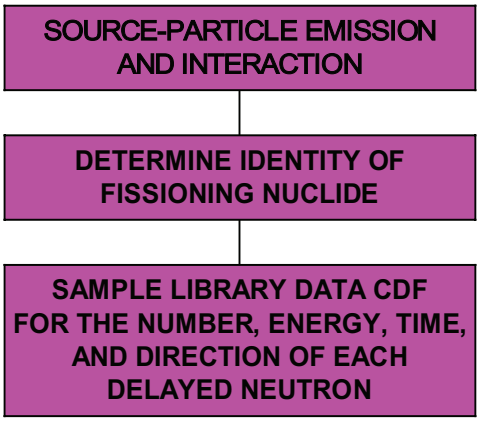

Figure 1. Schematic of the MCNP6 delayed-neutron production procedure for neutron-induced fission reactions using the library-data technique.

DN production using the library-data technique consists of three primary operations. The technique starts with source-particle emission and transport. For neutron-induced fission reactions, DN production is done using ACE library cumulative distribution

function (CDF) data. The ACE CDF data are used to determine the number, energy, emission time, and direction of each delayed neutron. This procedure is executed repeatedly until a sufficient number of source-particle histories have been executed to give statistically adequate results ("tallies").

4.2. DNDG model-physics procedure operation.

The physics-model technique discussed in Sections 2 and 3 can be used to produce DNDGs for fission and activation reactions. The general operation of this technique is illustrated in Fig. 2. The technique consists of five steps for delayed neutrons and gammas.

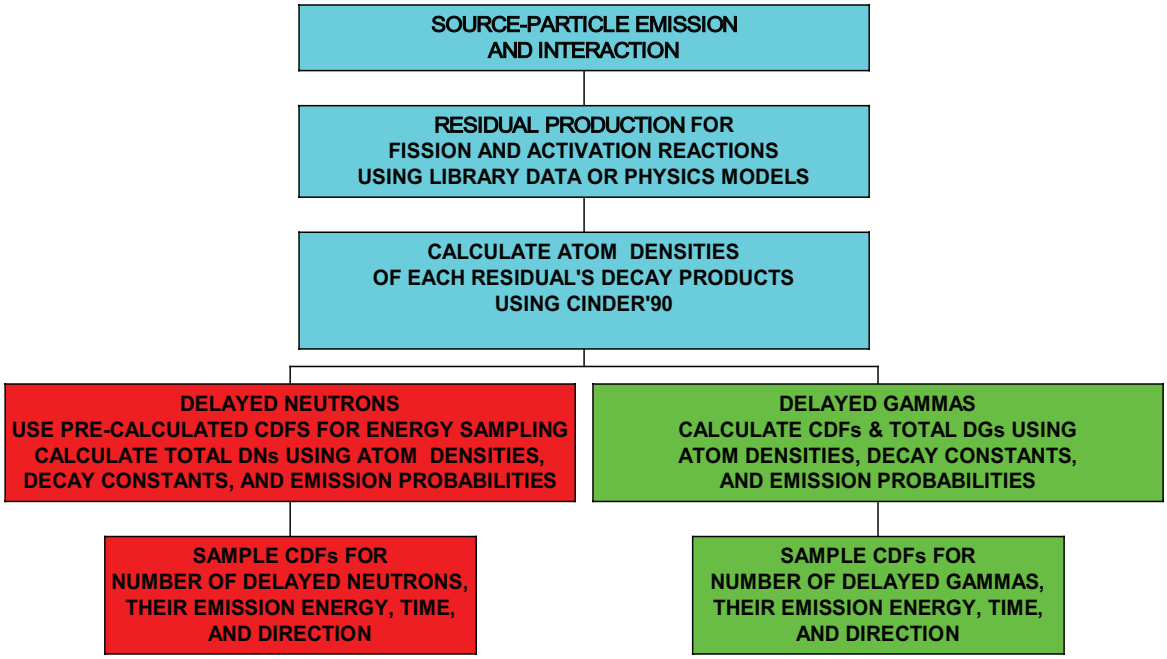

Figure 2. Schematic of the MCNP6 delayed-neutron and delayed-gamma production procedure for fission and/or activation reactions using the physics-model technique.

MCNP6 delayed-particle emission by the physics-model technique begins with source-particle emission and transport. This technique works with the large assortment of particle types treated by MCNP6. Reactions of source particles that cause fission and/or activation are candidates for delayed-particle production.

Second, the nuclear reaction by-products (residual nuclides) are determined for each fission or activation event. Depending on data availability,[*] users can request that this be done using library-data or physics-model techniques. Although library-data and physics-model naming conventions are used, the *residual*-production techniques should not be confused with the DNDG production techniques.

To illustrate, the residuals created by thermal-neutron fission of ^{235}U are determined by sampling the fission-yield curve for the fission products during a physics-model DN-production calculation. In contrast, residuals created by ^{235}U fission caused by 20-MeV neutrons can be sampled using fission-yield curve data or using model-physics results of the CEM code (Mashnik et al., 2008). Similarly, residual production by photofission of ^{239}Pu can be sampled using photofission-yield curve library data (Durkee et al., 2009c) or obtained using model results produced by CEM.

Third, after each residual nuclide is determined, its identity is sent to CINDER'90 (Wilson et al., 1995). CINDER'90 then generates the decay data for all of the radionuclides in the decay chain for a fission product. CINDER'90 is an isotopic transmutation code that calculates nuclide inventories in spatially homogeneous regions

[*] The available library data are described in the MCNP6 manual.

created by neutron transmutation and radioactive decay. Because the type and number of source and loss paths can vary from nuclide to nuclide, the corresponding differential equations can differ in structure, making a general solution difficult to obtain. CINDER'90 solves these equations using a decomposition scheme (England et al., 1976), wherein partial concentrations involve only a single-source term, but all loss mechanisms. The partial-concentration equations are described by a single set of coupled differential equations in which the uniform structure allows for a single analytic solution (assuming constant-flux conditions during a time increment). Once the partial concentrations are calculated, the total isotopic concentrations are calculated. CINDER'90 accommodates 3400 nuclides with atomic numbers (Z) ranging from 1 to 103. Originally written as a standalone code, CINDER'90 was been integrated into MCNPX to provide seamless simulation capability for delayed-particle emission calculations (Trellue et al., 2005). This capability is used in MCNP6.

Fourth, for DN production the pre-calculated CDFs discussed in Section 2 are used for energy sampling. For DG production, the atom densities, radioactive decay constants, and photon-emission probabilities of each unstable residual are used to calculate CDFs used for energy sampling. For DN and DG production, the atom densities, radioactive decay constants, and neutron- or photon-emission probabilities are used to calculate the total number of DNs and DGs created by a fission or activation event.

Fifth, the CDFs are sampled for DN and/or DG emission. For each delayed particle type, the number of particles to be emitted as well as the energy, time, and direction of

each delayed particle are calculated. Intra-cell densities are treated as constants, and isotropic DNDG emission is presumed.

Execution of this five-step procedure for DNDG emission is repeated until a sufficient number of source-particle histories have been executed to give statistically adequate tallies. Keeping in mind the data attributes discussed in Section 3 and the five primary procedure components discussed in this section, we next look at additional MCNP6 DN and DG attributes.

4.3. Additional DNDG physics-model attributes.

As was seen in Section 4.1, the MCNP6 library-data DN technique uses pre-calculated CDFs from ACE data. In contrast, as seen in Section 4.2 the MCNP6 physics-model DNDG procedure uses several operations to calculate CDFs. To speed execution it is desirable to reduce or eliminate repetitive calculations involved in CDF calculations for the physics-model technique.

We note that the physics-model DNDG procedure has the following interesting characteristic: any given problem has a limited number of fission products (FPs) or residuals. The development of the MCNP6 physics-model DNDG procedure has progressed with this characteristic in mind and with the objective of maximizing performance.

For simulations involving fission, keep in mind the classic double-hump fission yield curve (Lamarsh, 1972). Tests made using MCNP6 show that there are about 300–400 FPs that are sampled over 99% of the time. The remaining FPs are rarely sampled. This means that the CDFs developed for a particular DNDG simulation can be calculated once and stored for these frequently sampled FPs. These CDFs can then be accessed during subsequent particle histories. This calculation-and-storage strategy is efficient because the use of CINDER'90 and the execution of the nested DO loops that are required to calculate the CDFs are time consuming. We next consider important strategies that have been implemented to exploit this FP sampling characteristic.

The CDF calculation-and-storage strategy for DN emission using the CINDER'90 model technique is not a driving issue. The amount and fidelity of the DN emission data is relatively limited, so the DN CDFs can be calculated and stored without storage-limitation considerations.

The driving issue revolves around DG emission calculations. For DG calculations, users can request either low- or high-fidelity results. Low-fidelity simulations use 25-group multigroup (MG) data (contained in the cinder.dat file). MG DG simulations are useful for scoping analyses and basic DG signal detection. This type of simulation executes more quickly than high-fidelity simulations. For low-fidelity execution, only a single (MG) CDF integration strategy is used (Durkee et al., 2009a). Most modern computers can store the CDFs for all 3400 nuclides treated by CINDER'90, which

reduces execution time for simulations with fission and/or activation events by up to 99% versus calculations without CDF storage (Durkee et al., 2011).

High-fidelity DG simulations are more complicated. Recall from Section 3 that the line dataset (cindergl.dat) contains data for only 979 nuclides. For any fission or activation event, each residual and all of the unstable progeny may have line-emission data. However, instances can arise in which the residual(s) and/or any unstable progeny may not have line-emission data. In such instances, the MG data (cinder.dat) are used. Consequently, algorithms and infrastructure have been developed to treat hybrid CDFs consisting of line and MG components. For each fission or activation event, the CDF for each FP or residual can consist of all DG line data, all MG data, or a mixture of DG and MG data. The CDF integration scheme and storage strategy must accommodate these data issues (Durkee et al., 2009a).

Unfortunately, storage capacity on modern computers is inadequate to permit CDF storage for all residuals for line (high-fidelity) DG simulations. Fission or activation events can produce residuals and their decay progeny with thousands of emission lines. Thus, when considering that the CDFs for the residuals depend on the number of times (set to 100 in MCNP6) at which the atom densities are evaluated (using CINDER'90) and the number of emission lines, we see that arrays on the order of $3400 \times 100 \times 1000$ result (versus $3400 \times 100 \times 25$ for MG execution).[†] Two special techniques have been created to treat storage and execution issues for high-resolution DG simulations.

[†] High-fidelity simulations treating fission can have an even larger number of CDFs because of the need to treat pairs of fission products.

Because of the interest in active interrogation applications, the first high-resolution DG CDF storage strategy has been tailored to simulations involving thermal-neutron fission of ^{235}U and ^{239}Pu. MCNP6 calculations have been done to sample the most frequently sampled fission-product pairs for such simulations. These data are stored in MCNP6. CDFs are created and stored for the most frequently sampled FPs. CDFs for infrequently sampled FPs are repeatedly calculated. This strategy reduces execution time by well over 90% for the fission component of simulations with thermal-neutron fission of ^{235}U and ^{239}Pu. A future upgrade will be needed to extend the flexibility of this storage strategy to treat other fissioning nuclides, incident particle types, and energies.

Simulations with high-resolution DG production for residuals created by activation reactions can encompass a wide assortment of materials other than ^{235}U and ^{239}Pu. In the second storage technique, we have implemented an algorithm that dynamically determines the most frequently sampled individual activation products (APs). A list of these residuals is updated during execution for each activation event. CDFs for the most frequently sampled APs are stored for reuse. CDFs for less frequently sampled APs are calculated on an event-by-event basis. The dynamic-AP algorithm reduces execution time by 75% to well over 90% for most simulations (Durkee et al., 2011). A future upgrade will implement similar capability to treat pairs of APs.

In summary, for the physics-model technique DN treatment is not a driving issue in terms of storage. DG production can be executed for either low- or high-resolution

simulations. Low-resolution simulations execute relatively quickly, in large part because the CDFs for all residuals can be calculated once and stored for reuse. High-resolution DG simulations are storage intensive. Storage schemes have been developed to save CDFs for the most frequently sampled fission and activation products. CDFs for less frequently sampled residuals are recalculated each time such residuals are created. These schemes greatly reduce execution time and are transparent to the user.

5. COMPUTATIONAL RESULTS.

To illustrate the MCNP6 delayed-particle feature, we present results here for models based on experiments that were conducted by Beddingfield and Cecil (1998). In their experiments, highly enriched uranium (HEU) and Pu targets were irradiated by a moderated ^{252}Cf neutron source. Following irradiation, the targets were moved to an HPGe detector for high-resolution measurements of DG spectra. We have previously reported (Durkee et al., 2009b) simulation results based on their experiments. Because many of the details of their experiments were not provided, we approximated the experimental arrangement by using a 0.025-eV neutron pulse directed inwardly from a spherical surface source. In addition, because details of their HPGe detector were unavailable, we developed a simulated detector using representative parameters. Despite our modeling approximations, our simulation results yielded calculated spectra that agreed well with the measured data.

The published experimental results (Beddingfield and Cecil, 1998) were reported for the time windows (periods) 1050–1400 s and 1100–1450 s following fission for the HEU

and Pu experiments, respectively. Unpublished results from the same experiments for earlier and later measurement periods have been made available to us (Beddingfield, 2011). The measurement time windows are listed in Table 2. For convenience, we refer to the measurement periods as "Early," "Middle," and "Late." Measurement period Middle corresponds to the time reported in their published work (Beddingfield and Cecil, 1998) and in our earlier simulation work using MCNPX (Durkee et al., 2009b). Parameter "t_{cool}" is the time duration from the end of irradiation to the start of measurement, and "t_{meas}" is the duration of the measurement.

Table 2. Beddingfield and Cecil experimental measurement time data.

Measurement Period	HEU	Pu
	t_{cool},t_{meas} (s)	t_{cool},t_{meas} (s)
Early	563,33	600,35
Middle	1050,350	1100,350
Late	2560,830	2600,1000

We report here new results for MCNP6 simulations that have been executed using the Early, Middle, and Late measurement periods of Beddingfield and Cecil (1998) and Beddingfield (2011).

5.1. MCNP6 model of the Beddingfield and Cecil experiments.

The Beddingfield and Cecil (1998) experimental setups were approximated using two models: the first contained an HEU target, and the second a Pu target. Each target is a small disk with the same specifications as the experimental samples (descriptions are given in sections 5.1.1 and 5.1.2).

A two-part calculation was executed for each (HEU and Pu) model. Each calculation depicts 1) irradiation of a target followed by 2) placement of each target (individually) in a detector for measurement of the delayed-gamma emission. This two-part procedure is representative of the experimental procedure where targets were first irradiated and then moved to the HPGe detector.

Part one of the calculation simulated target irradiation. In the simulations, each disk was exposed to a 0.025-eV neutron pulse directed inwardly from a 2.7-cm radius spherical surface centered about the target. Delayed particles emitted during the measurement period were "recorded" using the MCNP6 surface-source feature.[†] This feature writes information (including emission time, energy, direction, location) about all particles—including delayed gammas and delayed neutrons—emitted in the time window for the Beddingfield measurements to a file ("surface source" file). In these calculations, the surface source recording location was the lower surface of the HEU or Pu disk target.

Following each irradiation calculation, the delayed-particle surface source was "moved" to our *in silico* HPGe detector to measure the delayed-gamma activity. The second-part (measurement) calculation transported the photons from the surface-source to

[†] The surface-source feature is standard with the general code release. A special modification writes the data to the surface-source file only for the stipulated time interval. A future code upgrade will permit automated treatment.

the detector. The MCNP6 "F8" pulse-height tally was used to simulate the detector response.*

Because the experimental detector design details are not available (Beddingfield and Cecil, 1998), the physical detector was modeled using the specifications given in Knoll (2000). The F8 tally uses the Gaussian energy broadening ("GEB") special feature ("FT"). The GEB feature simulates the peak-broadening effects exhibited by physical radiation detectors using the expression FWHM = $a + b\sqrt{E + cE^2}$, where E is the particle energy. For this study, the parameters (a, b, c) were (5.797×10^{-4} MeV, 7.192×10^{-4} MeV$^{1/2}$, 1.0 MeV^{-1}) ‡ (Princeton Gamma Tech, 2006).

Figure 3 illustrates the MCNP6 simulation models for the irradiation and detection calculations. In each part-one calculation, the disk-shaped target is irradiated by the inwardly directed neutron pulse emanating from a 2.7-cm-radius spherical surface surrounding the target. Delayed particles produced by fission and activation reactions in the target which reach the underside of the target during the measurement time windows are are recorded in a surface source file. In each part-two calculation, data from the surface-source file are read by MCNP6 and the delayed particles are transported in the HPGe detector. Separate calculations were executed for each measurement time.†

* The F8 (pulse-height) tally provides the energy distribution of pulses created in a cell that models a physical detector. The F8 energy bins correspond to the total energy deposited in a detector in the specified channels by each physical particle (history).

‡ The simulation used estimated values that should be representative of the Beddingfield and Cecil (1998) detector. The estimates were made using FWHM resolution at 0.122 and 1.33 MeV of 1 and 2 keV, respectively, presuming c=1.

† An upgrade to MCNP6 will be required to enable surface-source writing and reading for multiple time windows.

Calculation Part One: Target irradiation and
delayed-particle surface-source-file creation.

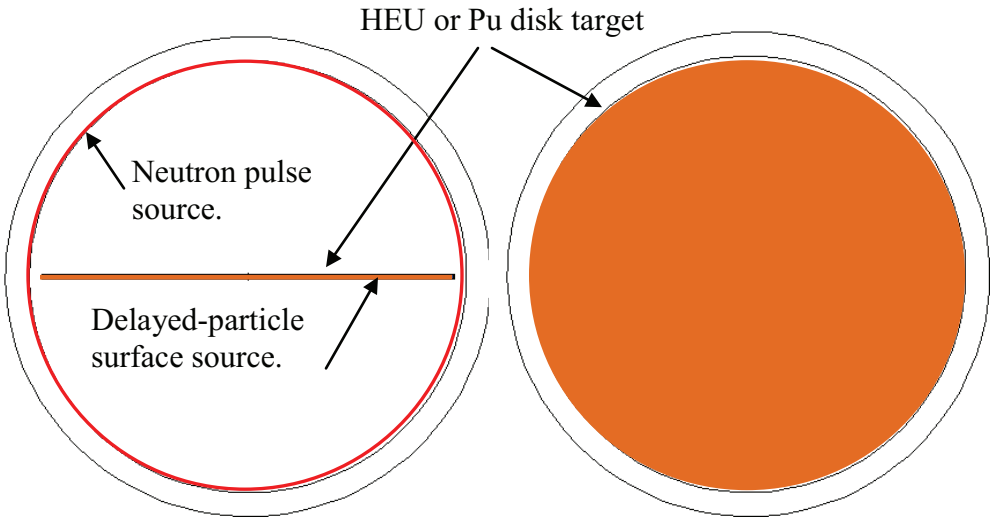

Calculation Part Two: Transport of delayed-particle surface source.

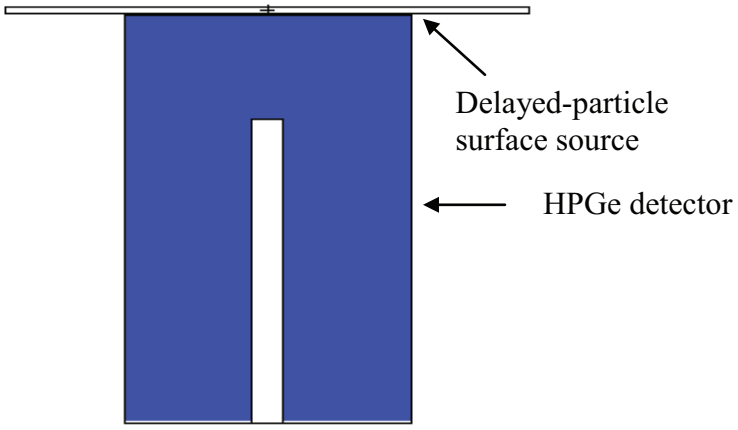

Figure 3. MCNP6 model approximating the Beddingfield and Cecil (1998) experimental setup. In each part-one calculation, a 0.025-eV neutron pulse is emitted inwardly from a 2.7-cm-radius spherical surface to induce fission in the HEU or Pu disk. Delayed particles emitted in the Early, Middle, or Late measurement time window after irradiation reaching the lower surface of the target are recorded in a surface-source file. In each part-two calculation, the surface source is read by MCNP6 and the delayed particles are transported to interact with the HPGe detector. Detector specs (radius = 1.4 cm, height = 4.50 cm) from Knoll (2000).

Simulations have been executed for each target to obtain DG data for the Early, Middle, and Late measurement periods. The simulations for each target and measurement period were done using two calculations that were designed to mimic the experimental procedure.

All irradiation calculations were executed using the MCNP6 physics-model DNDG production techniques with the high-fidelity DG CDF integration scheme to provide high-resolution results (sections 4.2 and 4.3). The Early calculation was executed using 100 million source histories, whereas the Middle and Late calculations were executed using 200 million source histories.[†] These quantities of histories enabled the 10 statistical tests to be passed for the total F8 tallies and gave reasonable statistics for the F8 pulse-height tallies for the part-two (measurement) calculations while giving reasonable qualitative agreement for the plotted spectra regarding the granularity of the experimental results.[*] The MCNP6 pulse-height tally calculations were obtained using 1-keV resolution (10^4 equal-width tally bins between 0 and 10 MeV)..

5.1.1. Uranium model.

The Beddingfield and Cecil (1998) uranium experiment consisted of a thin disk (5.08-cm diameter, 0.05588-cm thickness) of material consisting of 93.15 at.% ^{235}U and 6.85 at.% ^{238}U. The disk was exposed to a moderated ^{252}Cf source for 100 s. Following

[†] In addition, neutron transport was done using analog capture, rather than the default implicit capture for neutron transport, because the MCNP6 F8 pulse-height tally requires analog pulses. Execution also was done with fission and activation.

[*] The10 statistical checks provided by MCNP6 for the aggregate (all energy bins) F8 tally are passed. The relative uncertainties for all prominent peaks are < 0.10 and < 0.20 for the low-lying peaks.

irradiation, the sample was moved to an HPGe detector for DG measurement according to the data listed in Table 2.

Figure 4 shows the simulated and the previously reported experimental results (Beddingfield and Cecil, 1998) for the Middle measurement period. The lower section of Fig. 4 shows the calculated MCNP6 pulse-height tally.[†] The upper section of Fig. 4 shows the measured result (Beddingfield and Cecil, 1998, Fig. 2). The relative uncertainties of the MCNP6 results are less than 0.10/0.20 for the prominent/low-lying peaks. The MCNP6 results agree well with the results obtained using MCNPX (Durkee et al., 2009b).

Included in Fig. 4 are isotopic labels for several of the prominent lines. MCNP6 contains the capability to identify the emission lines in terms of the emitting nuclides.[*] As seen in Fig. 4, the identities of the radiating nuclides for the major lines identified by

---

[†] The MCNP6 output file ("outp") and tally data file ("mctal") F8 tally data have units of pulses/source particle-MeV. To normalize to fissions to obtain units of pulses/fission-MeV for plotting, the tally data are adjusted using the weight loss for fission (from the part-one calculation outp file summary table). For each HEU model, the weight loss for fission is 0.357 fissions/source particle. The tally multiplication factor for the HEU model is:
factor =f1photons/src part-MeV*1/(3.57d-1fiss/src part)=2.80 pulses/fiss-MeV

This factor was then used in the MCPLOT tally plot commands as "factor y" as

tal 858 noerr linlin xlims 0.8 1.55 ylims 0 ymax legend 1.4 lmax
fixed t=2 factor y 2.8 label "time"

where ymax=4e-3, 2e-2, and 2e-2, lmax=3.8e-3, 2.8e-2, and 2.8e-2, time=563–596s, 1050–1400s, and 2560–3390s for the Early, Middle, and Late HEU measurement periods, respectively.

[*] Future upgrades are required to provide a print table of associated peaks and nuclides and automated labeling of plotted spectra.However, the coding infrastructure that permits the association of the emission lines and the nuclides is in MCNP6 and was used to produce the results reported here.

MCNP6 are in agreement with most of those reported by Beddingfield and Cecil (1998) and Beddingfield (2009). However, there are some exceptions as noted in Table 3.[‡]

Table 3. Discrepancies between line identification for MCNP6 and measured data (Beddingfield and Cecil, 1998).

MCNP6		Measured	
Gamma Energy (MeV)	Emitting Nuclide(s)	Gamma Energy (MeV)	Emitting Nuclide(s)
0.8394	^{130}Sb+^{130m}Sb	0.8317	^{90}Rb+^{90m}Rb
0.8470	^{134}I	0.8394	^{130}Sb+^{130m}Sb
0.8840, 0.8844	^{134}I+^{104}Tc	0.8882	^{93}Sr
1.4359	^{138}Cs	1.4276	^{94}Sr
1.5247	^{146}Pr	1.5325	^{101}Mo
1.5325	^{101}Mo	unlabelled	unlabelled

[‡] For MCNPX results reported in Durkee et al., 2009b, the nuclides ^{130}Sb+^{130m}Sb were reported with typographical errors as ^{131}Sb+^{131m}Sb. Also, after further review, we concur with Beddingfield and Cecil that the first line above the ^{89}Rb 1.2481 MeV line is the 1.2604 MeV emission by ^{135}I. The ^{101}Mo emission at 1.2511 MeV contributes to the higher-energy portion of structure of the prominent peak that is labeled as ^{89}Rb.

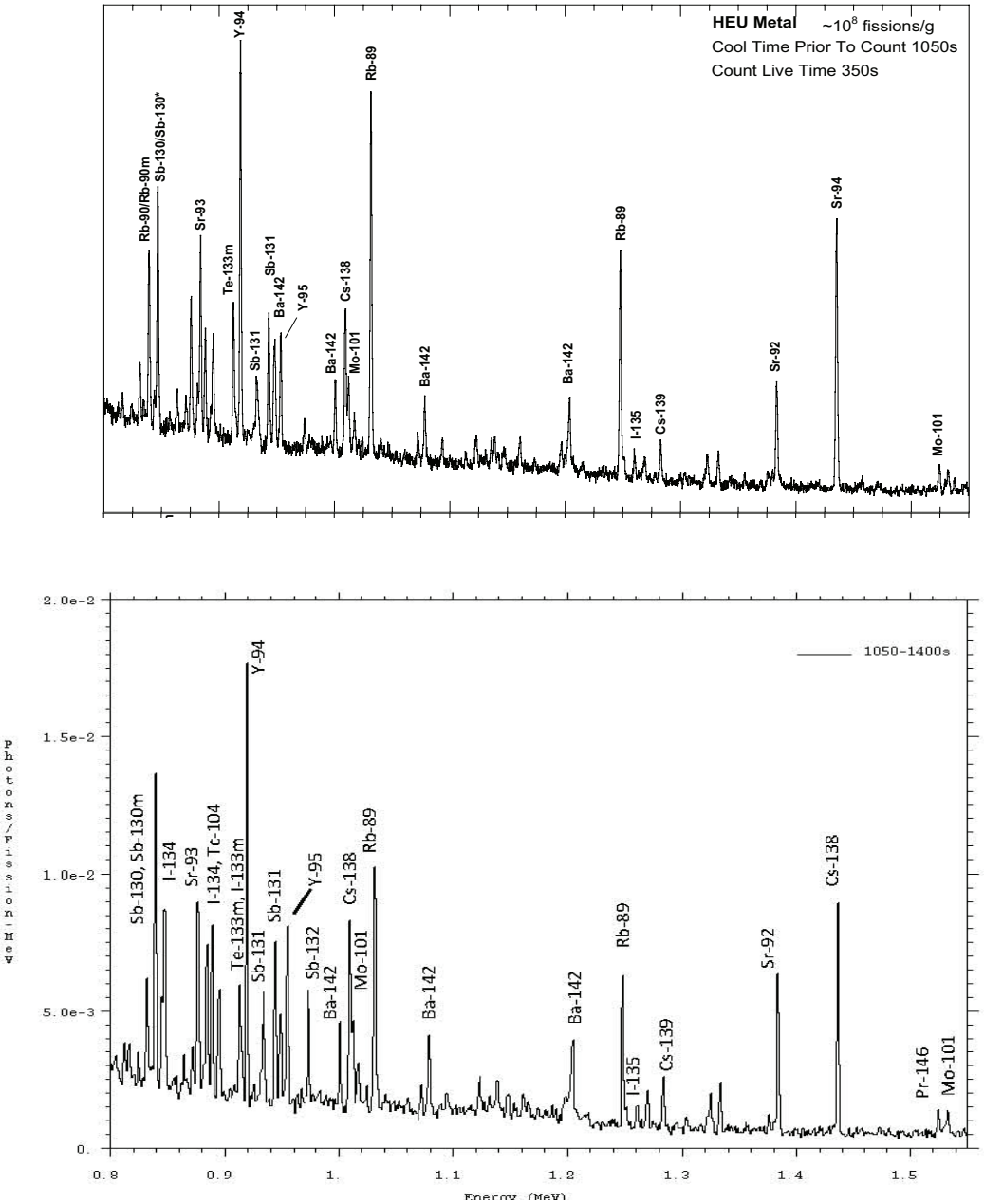

Figure 4. Middle measurement period: HEU delayed-gamma emission spectrum for 1050–1400 s. Lower: MCNP6 pulse-height ("F8") tally. Upper: Measured[†] (Beddingfield and Cecil 1998, Fig. 2, reprinted with permission).

[†] The published figure (Beddingfield, 1998) does not contain ordinate values. However, the ordinate values range between 0 and 2500 counts for a linear scale (Beddingfield, 2011).

Experimental data for the Early and Late measurement periods were not previously published (Beddingfield and Cecil, 1998). These data have been provided (Beddingfield, 2011) and are shown in the upper portions of Figs. 5 and 6 at Early and Late measurement times, respectively, for the energy range 0.8–1.55 MeV. The identities of the peaks at Early and Late measurement times are identical to those for the Middle time, so we present the results at Early and Late times without peak labeling to enhance the presentation of the spectra.

The lower portions of Figs. 5 and 6 are the spectra calculated using MCNP6. In general, the calculated and measured spectra are in good agreement for the Early and Late measurements.

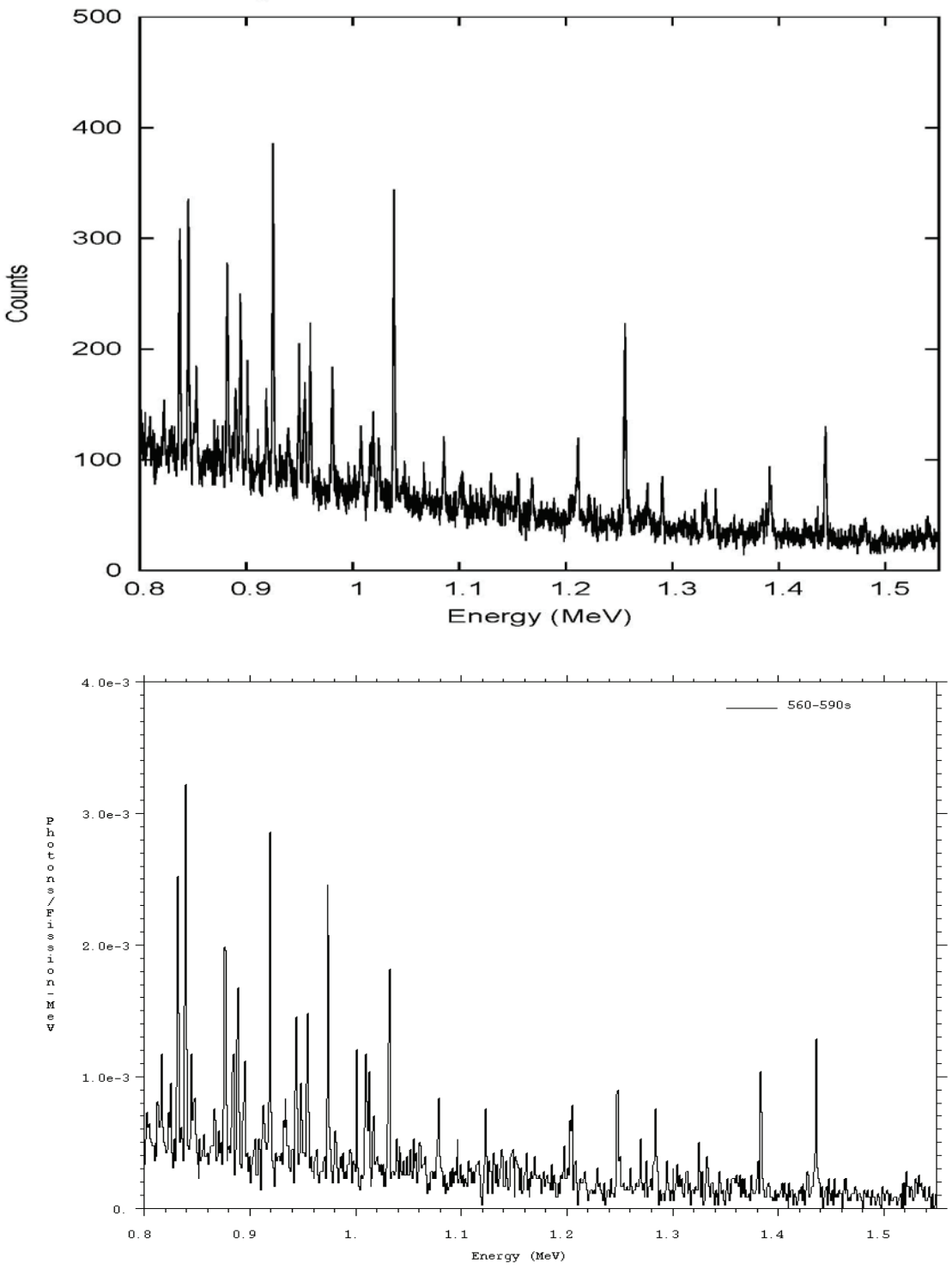

Figure 5. Early measurement period: HEU delayed-gamma emission spectrum for 563–596 s after irradiation. Lower: MCNP6 pulse-height ("F8") tally. Upper: Measured (Beddingfield, 2011).

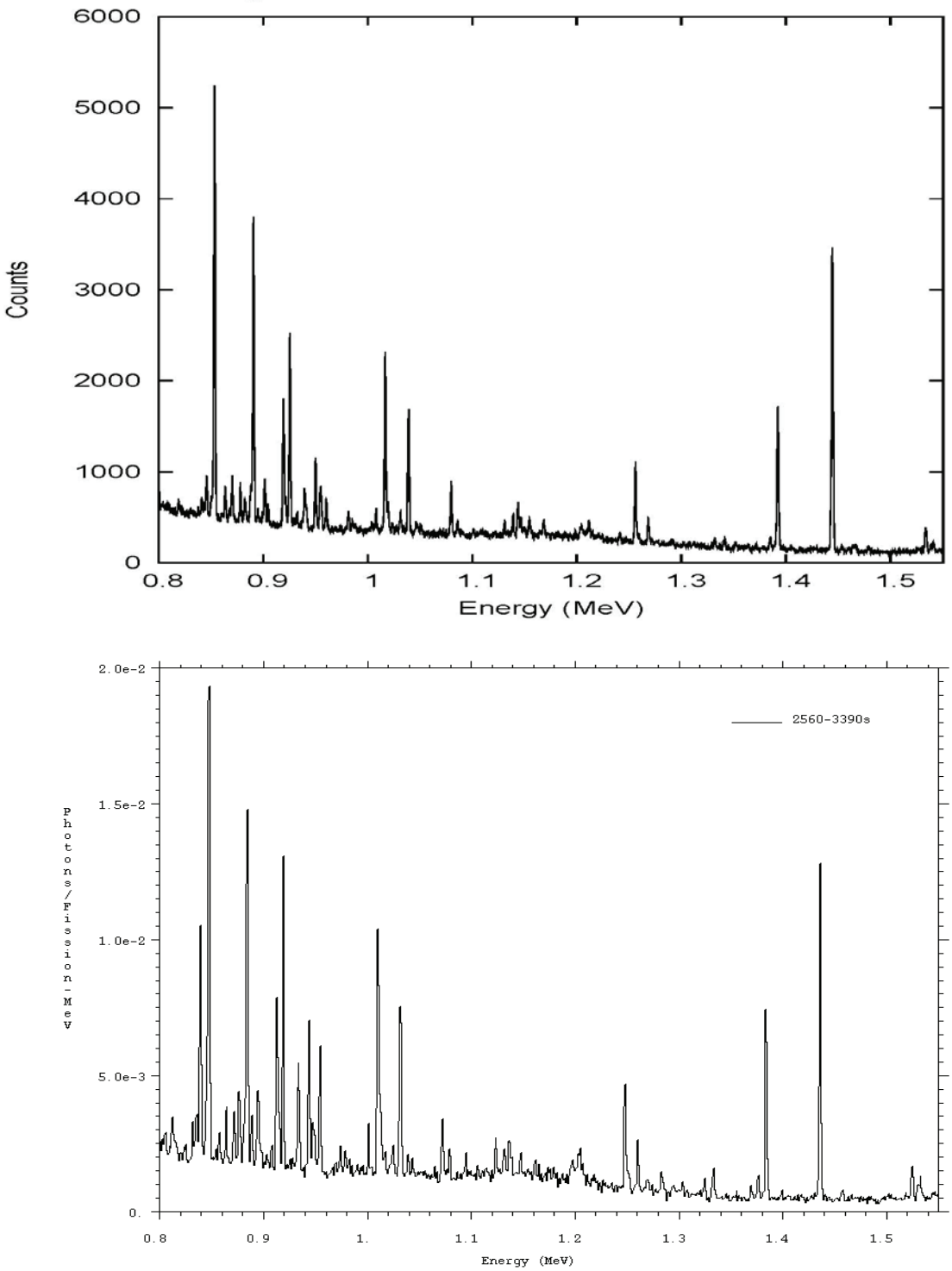

Figure 6. Late measurement period: HEU delayed-gamma emission spectrum for 2560–3390 s after irradiation. Lower: MCNP6 pulse-height ("F8") tally. Upper: Measured (Beddingfield, 2011).

Figures 4–6 show that HEU DG emission intensifies with time as the nuclides decay and strengthen DG production. The emission lines and general shape of the calculated and simulated spectra are in good agreement. The relative amplitude of the calculated spectra at the Late time are somewhat subdued relative to the Middle time as compared to the measured data. A discussion of factors impacting the results appears in Section 5.1.3.

The part-one irradiation simulations were executed using 72 2.4-GHz quad-processor nodes on a Linux cluster. The executable was made using an Intel FORTRAN 90 compiler and an MPI build. Execution CPU time requirements for the Early, Middle, and Late calculations were approximately 10 h, 29 h, and 22 h, respectively. The part-two measurement calculations were executed on a PC using a serial build and required only a few seconds of CPU time.

5.1.2. Plutonium model.

The Beddingfield and Cecil (1998) plutonium experiment closely resembles the uranium experiment. The plutonium disk (5.08-cm diameter, 0.05588-cm thickness) consisted of 98.97 at.% ^{239}Pu, 0.58 at.% ^{240}Pu, 0.0335 at.% ^{241}Pu, and 0.0179 at.% ^{242}Pu, and was clad with 0.0508-cm-thick copper. The sample was irradiated for 100 s using a moderated ^{252}Cf source. Following irradiation, the sample was moved to an HPGe detector for DG measurement according to the data listed in Table 2.

Figure 7 (lower) displays the calculated pulse-height tally.[†] The upper section of Fig. 7 shows the reported measured result (Beddingfield and Cecil 1998, Fig. 2). The simulated spectra are in good agreement with the experimental data, with the same peak identification exceptions as noted for ^{235}U.

[†] The MCNP6 "outp" file summary table indicates 0.306 fissions/source particle for each plutonium model simulation. The required MCPLOT tally multiplication factor "factor y" value and MCPLOT commands for the plutonium model are:
factor =f1photons/src part-MeV*1/(3.06d-1fiss/src part)=3.26 pulses/fiss-MeV

tal 858 noerr linlin xlims 0.8 1.55 ylims 0 ymax legend 1.35 lmax
fixed t=2 factor y 3.26 label "time"

where ymax=4e-3, 2e-2, and 3e-2, lmax=3.8e-3, 1.8e-2, and 2.8e-2, and time=600–635 s, 1100–1450 s, and 2600–3600 s for the Early, Middle, and Late measurement periods, respectively.

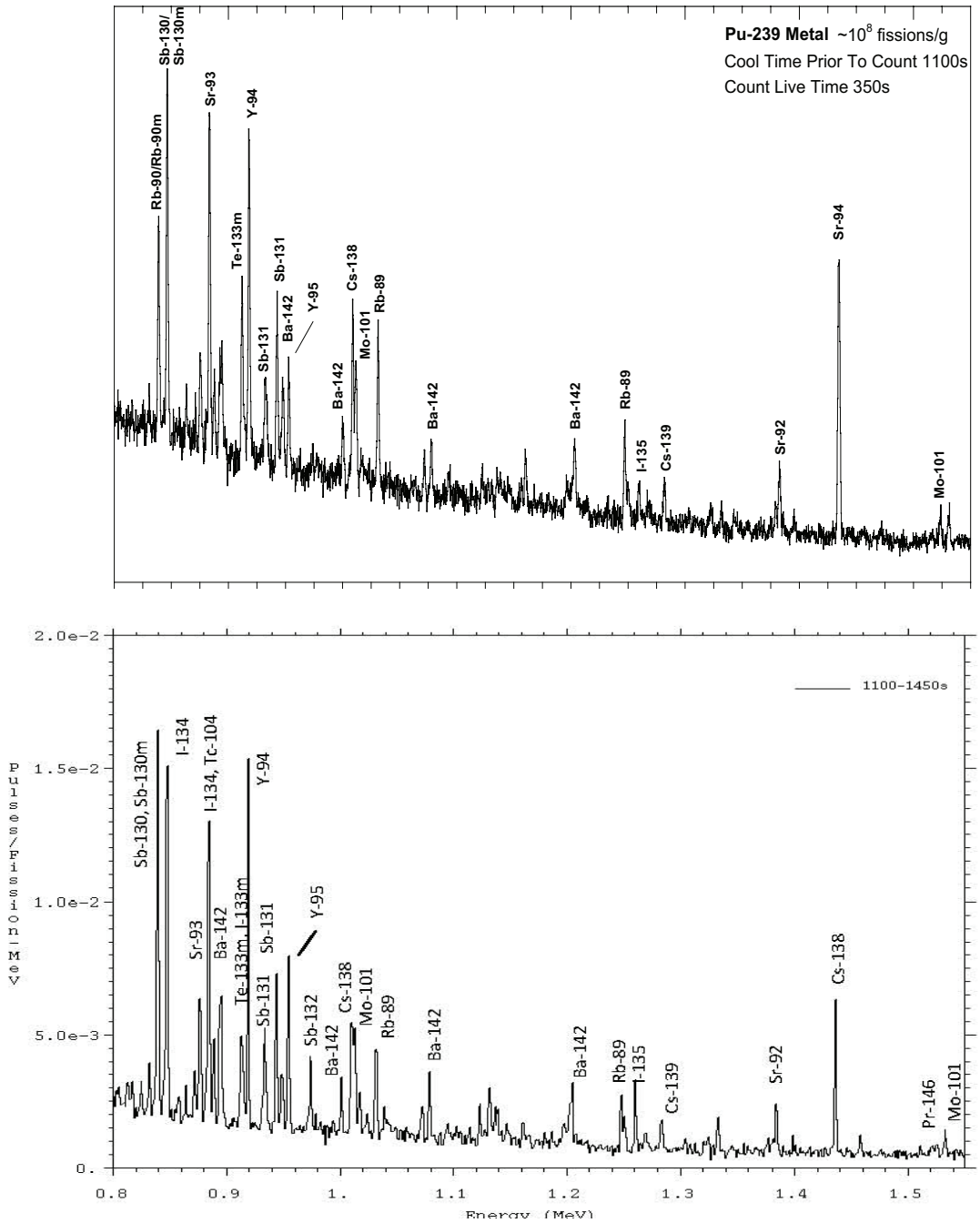

Figure 7. Middle measurement period: plutonium delayed-gamma spectrum for 1100–1450 s after irradiation. Lower: MCNP6 pulse-height (F8) tally. Upper: Measured[†] (Beddingfield and Cecil, 1998, Fig. 2, reprinted with permission).

[†] The published figure (Beddingfield, 1998) does not contain ordinate values. However,the ordinate values range between 0 and 1000 counts for a linear scale (Beddingfield, 2011).

Figures 8 and 9 show data at Early and Late measurement times (Beddingfield, 2011). The general structure of the calculated spectrum in Figs. 8 and 9 is in good agreement with the measured data.

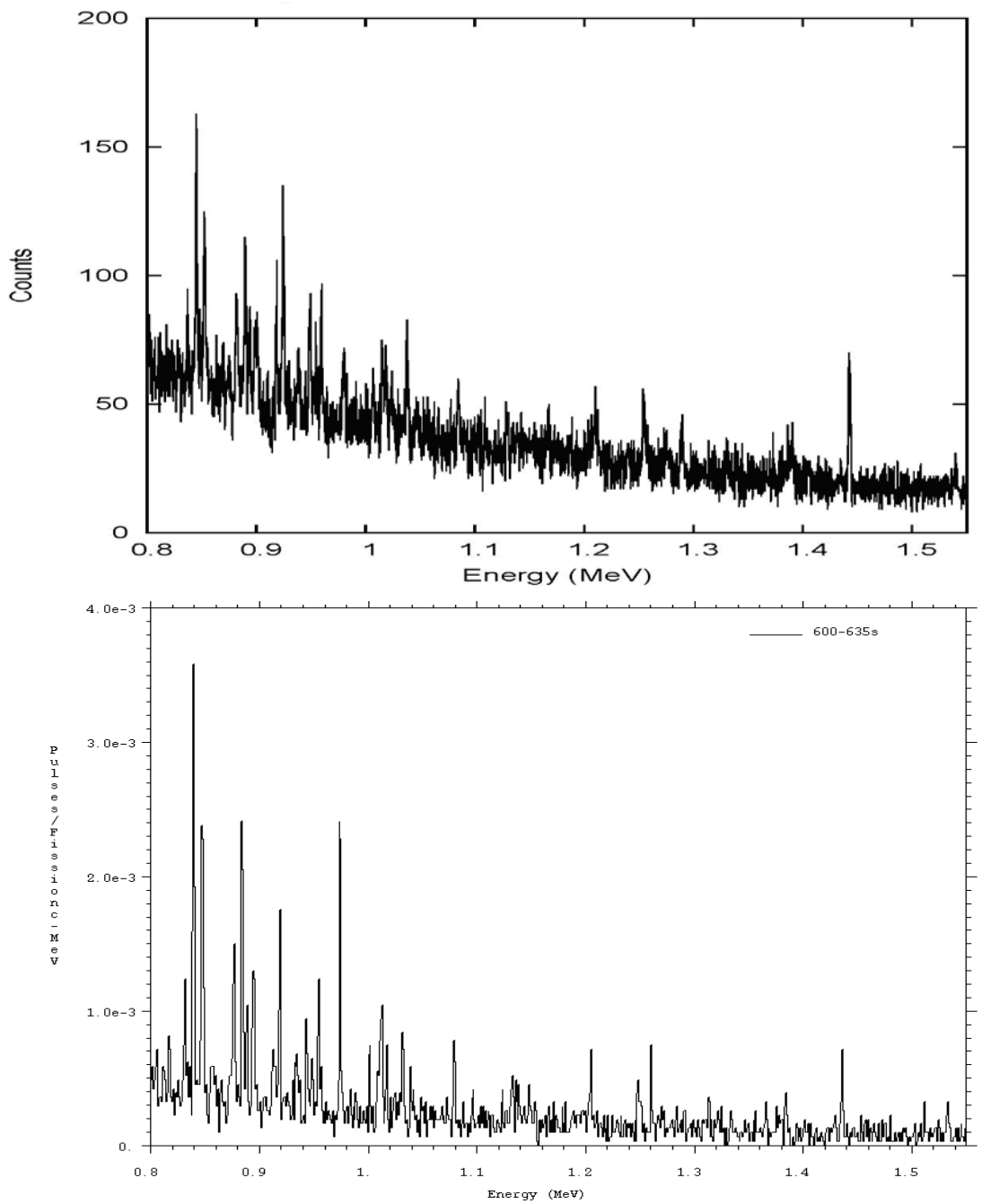

Figure 8. Early measurement period: plutonium delayed-gamma spectrum for 1100–1450 s after irradiation. Lower: MCNP6 pulse-height (F8) tally. Upper: Measured (Beddingfield, 2011).

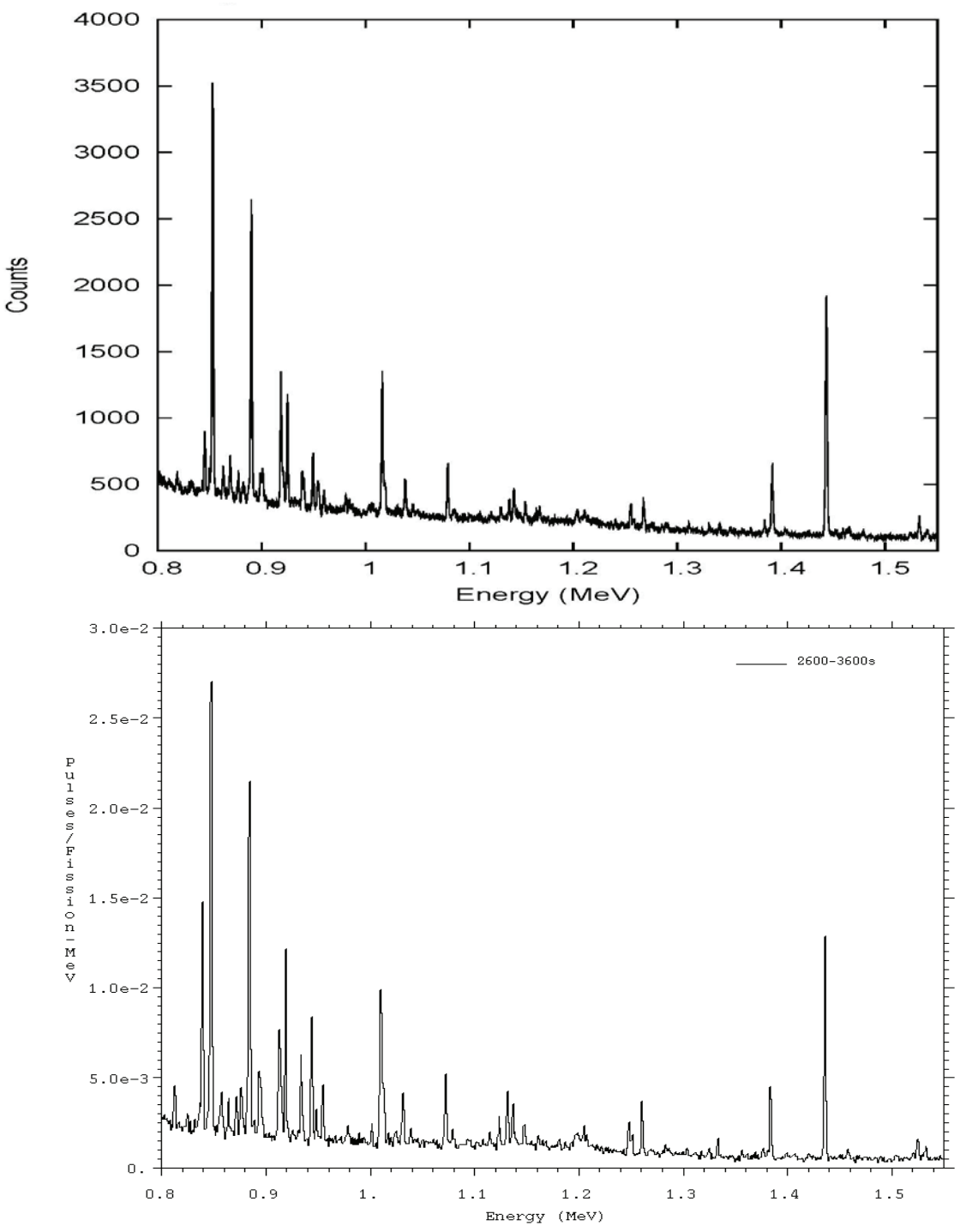

Figure 9. Late measurement period: plutonium delayed-gamma spectrum for 2600–3600 s after irradiation. Lower: MCNP6 pulse-height (F8) tally. Upper: Measured (Beddingfield, 2011).

These part-one irradiation simulations were executed using 72 2.4-GHz quad-processor nodes on a Linux cluster. The executable was made using an Intel FORTRAN 90 compiler and an MPI build. Execution CPU time requirements for the Early, Middle, and Late calculations were approximately 12 h, 33 h, and 26 h, respectively. The part-two measurement calculations were executed on a PC using a serial build and required only a few seconds of CPU time.

5.1.3. Observations regarding the calculated and experimental results.

In general, the calculated emission line structure concurs with the experimental data in the Early, Middle, and Late measurement periods. Some differences in the amplitudes of the peaks are observed and may be attributable to several experimental and computational factors, including the following:

- Energy resolution. The Gaussian broadening parameters for the MCNP6 calculations were deduced from PGT data (Princeton Gamma Tech et al., 2006) because experimental details were unavailable.
- MCNP6 tally energy-bin structure. A uniform 1-keV bin structure was used, which is representive of the average resolution for PGT HPGe detectors (Princeton Gamma Tech et al., 2006). The bin structure can cause tally spectra to differ from experimentally obtained spectra. For example, tally data can be recorded in two or more adjacent bins, which can tend to suppress the amplitude of a peak. Or, a single tally bin may have energy boundaries large enough to record more information than an experimental measurement.

- The detector response function. The MCNP6 model used only the Gaussian energy broadening function. The MCNP6 simulations do not treat detector response function details such as electron-hole formation and migration, loss in electronics, and photompltiplier tube behavior.
- Experimental mockup. The MCNP6 simulations were conducted using renditions of the targets to known specifications, but approximate representations of the irradiation and detection environments were modeled because many of the experimental details are unavailable (Beddingfield, 2006). Comparison of the simulated and experimental results show reasonable agreement, but precise correlation is not necessarily expected.
- MCNP6 CDF calculation. CDFs for energy and emission time include the use of the trapezoidal rule for the evaluation of the integral of time-varying atom densities (Durkee et al., 2009a). Thus, although the atom densities provided by CINDER'90 have analytic accuracy, the numerical evaluation of the integrals of the atom densities have errors. In general, quantification of the magnitude of these errors is difficult because of the complicated fission and activation-product nuclide chains. Assessment of the impact of the trapezoidal scheme on the results presented in this paper is difficult because, as discussed in Section 4, the appreciable storage needs for the CDFs do not readily allow for a refinement in the integration scheme parameters (time bins). An initial upgrade has been made to give analytic results for fission or activation products (Durkee et al., 2010). An improved integration scheme to treat the decay species of fission or activation products, with chains that can involve hundreds of nuclides, is pending.

- MCNP6 CDF sampling. As with all Monte Carlo simulations, all relevant CDFs must be adequately sampled so that the tally is statistically reliable. The DG CDF sampling includes emission as a function of energy, time (keeping in mind the time-dependent nature of the decay-chain atom densities), and direction. In its current state, MCNP6 permits only analog DG creation and transport.[‡] Thus, suitably converged results are obtained by running large numbers of source histories. Inadequate sampling can cause peak amplitudes to be unconverged. For these simulations, the necessary relative uncertainty and ten-statistical-check criteria were met.[†]
- MCNP6 energy-CDF data composition. The energy CDF is calculated for each fission or residual event using data for each principal residual and its radioactive progeny. As is discussed in Sections 3 and 4, the DG emission data is a key component of the energy CDF. Per Table 1, line-emission data are available for only 979 nuclides. The remainder of the emission data is multigroup. As noted in Section 4, the energy CDF for each fission or residual event can consist of line, multigroup, or a mixture of line and multigroup data components. The inclusion of multigroup data in an energy CDF degrades fidelity. Degradation is not deemed to be appreciable in our simulations, but can alter the calculated spectra. Until line data are available for all nuclides, it will be difficult to quantify the degree to which the hybrid CDFs degrade the calculated spectral resolution.

[‡] A future upgrade will be needed to bias delayed-gamma production.

[†] A tally is deemed to be questionable for a relative error of 0.1 to 0.2 and generally reliable for a relative error less than 0.1. Moreover, the MCNP6 ten statistical checks should be passed to further substantiate tally validity. However, the ten statistical checks are done for the aggragate tallies rather than for each peak.

- Atom density integration scheme. As alluded to in Section 4, calculation of the CDFs includes integrals (over time) of the time-dependent atom densities (Durkee et al., 2009; Durkee et al., 2011). For events with a single residual and no decay products, the integral is evaluated analytically. For residuals with unstable decay products, these integrals are evaluated using the trapezoidal rule. This numerical scheme produces varying degrees of error which will impact the CDF.
- Fission-yield data. The data of England and Rider (1994) are used in MCNP6. These consist of ENDF-B/VI data for a variety of nuclides and evaluations made using thermal ($E \leq 1$ eV), fission-spectrum (1 eV < E < 14 MeV), and high-energy (≥ 14 MeV) neutron spectra. The simulated spectra suggest that the fission-yield data are generally valid.

6. SUMMARY AND CONCLUSIONS.

There is an abundance of interest in delayed-neutron and -gamma (DNDG) radiation that is emitted as a result of the decay of radioactive species created by fission and activation processes. In recent years, this interest has been punctuated by homeland-security needs, for which active and passive interrogation techniques are being studied and deployed for the detection of explosives, chemical agents, and nuclear material.

Advances in computing have facilitated the use of the Monte Carlo technique to conduct highly detailed simulations. Modern personal computers permit Monte Carlo

calculations that were difficult to do on supercomputers 20 years ago, and low-cost Linux clusters facilitate highly detailed simulations in reasonable amounts of time.

In light of the interests in delayed-particle radiation and the advent of powerful computing platforms, work that began in 2004 has culminated in MCNP6 capability to execute automated Monte Carlo simulations of DNDG emission produced by radioactive species created by fission and activation reactions. DNDG simulations can be executed with a variety of options, including only DN or DG emission, concurrent DN and DG emission, and either low- or high-fidelity DG emission. Fission and activation residual production can be done using either extensive library data or physics packages that are included in MCNP6 for many types, energies, and combinations of source particles. Decay chains of fission and activation products are seamlessly calculated using CINDER'90. Model-dependent CDFs are calculated to enable simulation customization for a broad assortment of applications.

New validation calculations have been produced here for models based on the HEU and Pu neutron-induced fission experiments performed by Beddingfield and Cecil (1998). The MCNP6 results compare favorably with previously unpublished experimental results (Beddingfield, 2011). We emphasize that our validation assessments are illustrative of the MCNP6 delayed-particle feature rather than constituting stringent benchmarks because many of the aspects of the experimental work are unavailable (Beddingfield, 2006). Taken in this context, despite the approximations that were made with the MCNP6 modeling, the simulated and experimental results are in reasonable agreement. We

encourage the execution of detailed experimental endeavors as an avenue for further validation benchmarking.

The MCNP6 delayed-particle feature has been developed for simulations with radiation sources. That is, this feature is designed to execute source (SDEF) simulations. Future work will be required to enable criticality (kcode) simulations with delayed-particle emission. Additional future improvements will include tabulated output of associated DG emission lines and nuclides, automated annotation of DG emission peaks for spectral plots, an improved CDF nuclide-density time-integration scheme, and user-friendly surface-source time windowing. Work is currently underway to provide delayed beta emission (McKinney, 2012).

The MCNP6 delayed-particle feature provides DNDG simulation capability that should be of interest in many areas. Such areas include homeland security interrogation, health physics, sensor protection, waste characterization, radioanalytical chemistry, environment, health, medicine, nutrition, geology, and material science.

ACKNOWLEDGEMENTS

We gratefully acknowledge the support of DHS/DNDO and appreciate the experimental data provided by David Beddingfield.

REFERENCES

Ayranov M. and Schumann D., "Preparation of ^{26}Al, ^{59}Ni, ^{44}Ti, ^{53}Mn and ^{60}Fe From a Proton Irradiated Copper Beam," *J. Radioanalytical Nuclear Chemistry*, **286**, 649–654 (2010).

Barzilov A.P., Novikov I.S., and Cooper B., "Computational Study of Pulsed Neutron Induced Activation Analysis of Cargo," *J. Radioanalytical Nuclear Chemistry*, **282**, 177–181 (2009).

Beddingfield D.H. and Cecil F.E., "Identification of Fissile Materials From Fission Product Gamma-Ray Spectra," *Nuclear Instruments and Methods in Physics Research A*, **417**, 405–412 (1998).

Beddingfield D.H., private communication (2006).

Beddingfield D.H., private communication (2011).

From Cardinals to Chaos—Reflections on the Life and Legacy of Stanislaw Ulam, Cambridge University Press, Cooper N.G., Ed., New York (1989).

Chichester D.L. and Seabury E.H.. "Using Electronic Neutron Generators in Active Interrogation to Detect Shielded Fissonable Material," *IEEE Transactions on Nuclear Science*, **56**(2), 441–447 (2009).

de Hoffmann F. (April 6, 1945), "Delayed Neutrons From 25 After Short Irradiation," Los Alamos National Laboratory report LA-252.

de Hoffmann F., Feld B.T., and Stein P.R. (November 15, 1948), "Delayed Neutrons From U^{235} After Short Irradiation," *Physical Review*, **74**, no. 10, 1330–1337.

Dighe P.M., Berthoumieux E., Dore D., Laborie J.M., Ledoux X., Macary V., Panebianco S., and Ridikas D., "Delayed Gamma Studies From Photo-Fission of ^{237}Np for Nuclear Waste Characterization," *Annals of Nuclear Energy*, **36**, 399–403 (2009).

Dore D., David J.C., Giacri M.L., Laborie J.M., Ledoux X., Petit M., Ridikas D., and van Lauwe A., "Delayed Neutron Yields and Spectra from Photofission of Actinides with Bremsstrahlung Photons Below 20 MeV," *J. of Physics: Conference Series* **41**, 241–247 (2006).

Durkee J.W., Jr., James M.R., McKinney G.W., Trellue H.R., Waters L.S., and Wilson W.B., "Delayed-Gamma Signature Calculation for Neutron-Induced Fission and Activation Using MCNPX, Part I: Theory," *Progress in Nuclear Energy*, **51**, 813–827 (2009a).

Durkee Joe W., Jr., McKinney Gregg W., Trellue Holly R., Waters Laurie S., and Wilson W.B., "Delayed-Gamma Simulation Using MCNPX. Part II: Simulations," *Progress in Nuclear Energy*, **51**, 828-836 (2009b).

Durkee Joe W., Jr., McKinney Gregg W., Trellue Holly R., Waters Laurie S., and Wilson W.B., "Delayed-Gamma Simulation Using MCNPX," *J. Nuclear Technology*, **168**, 761–764 (2009c).

Durkee Joe W., Jr., James Michael R., McKinney Gregg W., and Waters Laurie S., "MCNPX Delayed-Gamma Feature Enhancements," Transactions of the American Nuclear Society, **103**, 651–652 (2010).

England T.R., Wilson W.B., and Stamatelatos M.G. (December 1976), "Fission Product Data for Thermal Reactors. Part 1: A Data Set for EPRI-CINDER Using ENDF/B-IV," Los Alamos National Laboratory report LA-6745-MS.

England T.R. and Rider B.F. (October, 1994), "Evaluation and Compilation of Fission Product Yields," Los Alamos National Laboratory report LA-UR-94-3106.

Fei T., Dehong L., Fengqun Z., Junhua L., Hua T., and Xiangzhong K, "Determination of Trace Elements in Chinese Medicinal Plants by Instrumental Neutron Activation Analysis," *J. Radioanalytical Nuclear Chemistry*, **284**, 507–511 (2010).

Frontasyeva M.V., Pavlov S.S., and Shvetsov V.N., "NAA for Applied Investigations at FLNP JINR: Present and Future," *J. Radioanalytical Nuclear Chemistry*, **286**, 519–524 (2010).

Goorley T., James M., Booth T., Brown F., Bull J., Cox L.J., Durkee J., Elson J., Fensin M., Forster R.A., Hendricks J., Hughes H.G., Johns R., Kiedrowski B., Martz R., Mashnik S., McKinney G., Pelowitz D., Prael R., Sweezy J., Waters L., Wilcox T., and Zukaitis T., "Initial MCNP6 Release Overview," *J. Nuclear Technology*, submitted December 2011.

Goudsmit S.A., *ALSOS*, Tomash Publishers, American Institute of Physics, p. 13 (1988).

Gozani T., "Fission Signatures for Nuclear Material Detection," *IEEE Transactions on Nuclear Science*; **56**, no.3, 736–741 (June 2009).

Guung T-C, Tsai W-F, Kuo W-S, and Chen, J-S, "MCNP Simulation of TRR-II Cold Neutron Source Design," *Physica B*, **311**, 158–163 (2002).

Henderson D.L., Sawan M.E., Moses G.A., "Radiological Dose Calculations for the Diode Region of the Light Ion Fusion Target Development Facility," *Fusion Technology*, **13**, 594–615 (1988).

Hollas C.L., Close D.A., and Moss C. E., "Analysis of Fissionable Material Using Delayed Gamma Rays from Photofission," *Nuclear Instruments and Methods in Physics Research Section B: Beam Interactions With Materials and Atoms*, **24-25**, Supplement Part 1, pp. 503–505 (April 1987).

Katakura J. and England T.R., "Augmentation of ENDF/B Fission Product Gamma-Ray Spectra by Calculated Spectra," Los Alamos National Laboratory report LA-12125-MS (1991).

Kawano T., Moller P., and Wilson W.B., "Calculation of Delayed-Neutron Spectra in a Quasiparticle Random-Phase Approximation–Hauser-Feshbach Model," *Physical Review C,* **78**, pp.054601-1–0546018 (2008).

Kawano T., personal communication (2011).

Lamarsh J.R., *Introduction to Nuclear Reactor Theory*, Addision-Wesley Publishing Company, Inc., Reading, Massachusetts, 92–94 (1972).

Liew S.L. and Ku L.P., "Monte Carlo Calculation of Delayed Gamma Dose Rate in Complex Geometry Using the Concept of Effective Delayed Gamma Production Cross Section," *Nuclear Science and Engineering*, **107**, 114–130 (1991).

Ma R., Zhao X., Rarback H.M., Yasumura S., Dilmanian F.A., Moore R.I., Lo Monte A.F., Vodopia K.A., Liu H.B., Economos C.D., Nelson M.E., Aloia J.F., Vaswani A.N., Weber D A., Pierson R.N. Jr., and Joel D.D., "Calibration of the Delayed-Gamma Neutron Activation Facility," *Medical Physics*, **23**, no.2, 273–277 (February, 1996).

Mashnik S. G., Gudima K. K., Prael R. E., Sierk A. J., Baznat M. I., and Mokhov N. V., "CEM03.03 and LAQGSM03.03 Event Generators for the MCNP6, MCNPX, and MARS15 Transport Codes," invited lectures presented at the Joint ICTP-IAEA Advanced Workshop on Model Codes for Spallation Reactions, February 4–8, 2008, ICTP, Trieste, Italy, Los Alamos National Laboratory report LA-UR-08-2931 (2008); E-print: arXiv:0805.0751v2 [nucl-th]; IAEA Report INDC(NDS)-0530, Vienna, Austria, August 2008, p. 53.

McKinney Gregg W., "MCNP6 Enhancements of Delayed-Particle Production," *PHYSOR 2012 – Advances in Reactor Physics.*, Knoxville, Tennessee, USA, April 15-20, American Nuclear Society.

Moon P.B. (April 7, 1945), "Short-Period Delayed Gammas From Fission of 25," Los Alamos National Laboratory report LA-253.

Morgan K.Z. and Turner J.E., *Principles of Radiation Protection*, Robert E. Krieger Publishing Company, Huntington, New York, 31–49 (1973).

Norman E.B., Prussin S.G., Larimer R., Shugart H., Browne E., Smith A.R., McDonald R.J., Nitsche H., Gupta P., Frank M.I., and Gosnell T.B., "Signatures of Fissile Materials:

High-Energy γ Rays Following Fission**,**" *Nuclear Instruments and Methods in Physics Research A*; **521**, 608–610 (2004).

"MCNPX User's Manual Version 2.7.0," Los Alamos National Laboratory report LA-CP-11-00438, Pelowitz D.B., ed., (April 2011).

Pruet J., Hall J., Descalle M.A., and Prussin S., "Monte Carlo Models for the Production of β -Delayed Gamma-Rays Following Fission of Special Nuclear Materials**,**" *Nuclear Instruments and Methods in Physics Research B*; **222**, 403–410 (2004).

Richtmyer R.D. and von Neumann J., "Statistical Methods in Neutron Diffusion," Los Alamos National Laboratory report LAMS-551 (April 9, 1947).

Roberts R.B., Meyer R.C., and Wang P., "Further Observations on the Splitting of Uranium and Thorium**,**" *Physical Review*; **55**, 510–511 (1939).

Siciliano E.R., Ely J.H., Kouzes R.T., Milbrath B.D., Schweppe J.E., and Stromswold D.C., "Comparison of PVT and NaI(Tl) Scintillators for Vehicle Portal Monitor Applications," *Nuclear Instruments and Methods in Physics Research A*; **550**, 647–674 (2005).

Slaughter D.R., Accatino M.R., Bernstein A., Dougan A.D., Hall J.M., Loshak A., Manatt D.R., Pohl B.A., Walling R.S., Weirup D.L., and Prussin S.G., "The 'Nuclear Car Wash': A Scanner to Detect Illicit Special Nuclear Material in Cargo Containers," *IEEE Sensors Journal*; **5**, no. 4, 560–564 (August, 2005).

Spletzer B.L., "The Delayed Gamma Environment Produced by Exoatmospheric Nuclear Weapons Detonation (U)," Sandia Report SAND91-0285 (1992).

Sterbentz J.W., Jones J.L., Yoon W.Y., Norman D.R., and Haskell K.J., "Benchmark Validation Comparisons of Measured and Calculated Delayed Neutron Detector Responses for a Pulsed Photonuclear Assessment Technique," *Nuclear Instruments and Methods in Physics Research B*; **261**, 373–377 (2007).

Szasz F.M., *The Day the Sun Rose Twice*, University of New Mexico Press, Albuquerque, 115–144 (1984).

Trellue H.R., McKinney G.W., and Durkee J., "Burnup Capability Added to MCNPX," American Nuclear Society 2005 Annual Meeting (2005).

Weidenspointner G., Harris M. J., Sturner S., and Teegarden B.J., "MGGPOD: A Monte Carlo Suite for Modeling Instrumental Line and Continuum Backgrounds in Gamma-Ray Astronomy**,**" *The Astrophysical Journal Supplement Series*, **156**, 69–91 (January, 2005).

Wilson W.B., England T.R., George D.C., Muir D.W., and Young P.G. (1995), "Recent Development of the CINDER'90 Transmutation Code and Data Library for Actinide Transmutation Studies," Los Alamos National Laboratory report LA-UR-2181.

LIST OF TABLE CAPTIONS

Table 1. Line-data composition for 979-radionuclide delayed-gamma dataset.

Table 2. Beddingfield and Cecil experimental measurement time data.

Table 3. Discrepancies between line identification for MCNP6 and measured data (Beddingfield and Cecil, 1998).

LIST OF FIGURE CAPTIONS

Figure 1. Schematic of the MCNP6 delayed-neutron production procedure for neutron-induced fission reactions using the library-data technique.

Figure 2. Schematic of the MCNP6 delayed-neutron and delayed-gamma production procedure for fission and/or activation reactions using the physics-model technique.

Figure 3. MCNP6 model approximating the Beddingfield and Cecil (1998) experimental setup. In each part-one calculation, a 0.025-eV neutron pulse is emitted inwardly from a 2.7-cm-radius spherical surface to induce fission in the HEU or Pu disk. Delayed particles emitted in the Early, Middle, or Late measurement time window after irradiation reaching the lower surface of the target are recorded in a surface-source file. In each part-two calculation, the surface source is read by MCNP6 and the delayed particles are transported to interact with the HPGe detector. Detector specs (radius = 1.4 cm, height = 4.50 cm) from Knoll (2000).

Figure 4. Middle measurement period: HEU delayed-gamma emission spectrum for 1050–1400 s. Lower: MCNP6 pulse-height ("F8") tally. Upper: Measured[†] (Beddingfield and Cecil 1998, Fig. 2, reprinted with permission).

Figure 5. Early measurement period: HEU delayed-gamma emission spectrum for 563–596 s after irradiation. Lower: MCNP6 pulse-height ("F8") tally. Upper: Measured (Beddingfield, 2011).

Figure 6. Late measurement period: HEU delayed-gamma emission spectrum for 2560–3390 s after irradiation. Lower: MCNP6 pulse-height ("F8") tally. Upper: Measured (Beddingfield, 2011).

Figure 7. Middle measurement period: plutonium delayed-gamma spectrum for 1100–1450 s after irradiation. Lower: MCNP6 pulse-height (F8) tally. Upper: Measured[†] (Beddingfield and Cecil, 1998, Fig. 2, reprinted with permission).

Figure 8. Early measurement period: plutonium delayed-gamma spectrum for 1100–1450 s after irradiation. Lower: MCNP6 pulse-height (F8) tally. Upper: Measured (Beddingfield, 2011).

[†] The published figure (Beddingfield, 1998) does not contain ordinate values. However, the ordinate values range between 0 and 2500 counts for a linear scale (Beddingfield, 2011).

[†] The published figure (Beddingfield, 1998) does not contain ordinate values. However,the ordinate values range between 0 and 1000 counts for a linear scale (Beddingfield, 2011).

Figure 9. Late measurement period: plutonium delayed-gamma spectrum for 2600–3600 s after irradiation. Lower: MCNP6 pulse-height (F8) tally. Upper: Measured (Beddingfield, 2011).